J Math Chem (2012) 50:2558–2576
DOI 10.1007/s10910-012-0049-z

ORIGINAL PAPER

Magnetic resonance spectroscopy with high-resolution and exact quantification in the presence of noise for improving ovarian cancer detection

Dževad Belkić · Karen Belkić

Received: 30 May 2012 / Accepted: 4 July 2012 / Published online: 24 July 2012

Abstract Ovarian cancer is the most common cause of death from gynecological malignancies in many developed countries. When confined to the ovary, the 5-year survival rates are over 90 %, but detection methods are insufficiently accurate for widespread application. Consequently, ovarian cancer is typically diagnosed late, with poor prognosis. Magnetic resonance spectroscopy (MRS) could potentially improve ovarian cancer diagnosis, but is currently hampered by poor resolution for this small, moving organ. Advanced signal processing methods through the fast Padé transform (FPT) can improve resolution and provide quantitative metabolic information. We applied the FPT to noise-corrupted time signals generated according to in vitro MRS data as encoded from malignant ovarian cyst fluid. In the presence of background noise, the FPT converged using merely 1/8 of the full signal length $N = 1024$, amounting to some 128 data points. This number of time signal points permits reconstruction of altogether 128 spectral parameters for 64 ensuing resonances. Each resonance is quantified by 2 spectral parameters, the complex-valued frequencies and amplitudes. The FPT accurately reconstructed the spectral parameters for all twelve genuine resonances from which the input time signal is intrinsically built. Thereby, in the presence of noise, the FPT provided fully reliable estimates of metabolite concentrations characteristic of malignant ovarian cyst fluid. Through the practical concept of signal-noise separation

Dž. Belkić (✉) · K. Belkić
Department of Oncology-Pathology, Karolinska Institutet, Building P-9, 2nd floor, Box 260, 17176 Stockholm, Sweden
e-mail: Dzevad.Belkic@ki.se

K. Belkić
School of Community and Global Health, Claremont Graduate University, Claremont, CA, USA

K. Belkić
Institute for Prevention Research, University of Southern California School of Medicine, Los Angeles, CA, USA

by means of so-called pole-zero cancellations (Froissart doublets), the remaining 52 resonances from the total of 64 resonances were unequivocally identified as spurious and, as such, could confidently be discarded. Given that magnetic resonance-based modalities entail no exposure to ionizing radiation, if their diagnostic accuracy were improved, magnetic resonance imaging and spectroscopy could have broader applications in screening surveillance for early ovarian cancer detection, especially among women at high risk. The present results suggest that Padé-optimized MRS could help achieve that goal.

Keywords Magnetic resonance spectroscopy · Mathematical optimization · Ovarian cancer · Gaussian noise

Abbreviations

Ala	Alanine
au	Arbitrary units
CF	Continued fractions
Cho	Choline
Cr	Creatine
Crn	Creatinine
FFT	Fast Fourier transform
FID	Free induction decay
FPT	Fast Padé transform
Glc	Glucose
Gln	Glutamine
IFPT	Inverse fast Padé transfor
Iso	Isoleucine
Lac	Lactate
Lys	Lysine
Met	Methionine
MR	Magnetic resonance
MRI	Magnetic resonance imaging
MRS	Magnetic resonance spectroscopy
ppm	Parts per million
RMS	Root-mean-square
SNR	Signal-to-noise ratio
TVUS	Transvaginal ultrasound
Val	Valine
ww	Wet weight

1 Introduction

1.1 The clinical problem: the lack of accurate early detection of ovarian cancer

Ovarian cancer is the 7th leading cause of cancer deaths among women worldwide [1]. In many developed countries, it is the most common cause of death from gyneco-

logical malignancies [2]. This malignancy is most often detected after spread beyond the true pelvis, when the prognosis is very poor, whereas stage Ia disease has better than a 90 % chance of 5-year survival. Unfortunately, early detection is still beyond current reach with standard diagnostic methods. Consequently, despite progress in treatment, mortality rates from ovarian cancer have not declined substantially over the last 30 years [3].

Albeit sensitive, transvaginal ultrasound (TVUS) lacks adequate specificity to distinguish benign from malignant adnexal changes [4]. Ovarian cancer can be detected more accurately by magnetic resonance imaging (MRI). In a meta-analytical comparison of morphological imaging modalities, MRI was of greatest incremental value in identifying ovarian cancer when the nature of adnexal mass was considered uncertain on TVUS [5]. Nevertheless, even with contrast-enhanced MRI, sixty of 241 (24.9 %) false positive findings from initial TVUS were not recognized as benign lesions [5].

Magnetic resonance spectroscopy (MRS) could potentially enhance the specificity of MRI by detecting metabolic features characteristic of ovarian cancer. Since molecular changes often precede morphologic alterations, MRS might further improve sensitivity, as well. However, in a recent review of the published studies, in vivo MRS was not found to adequately distinguish malignant from benign ovarian lesions [6]. Poor resolution and signal-to-noise ratio (SNR) have been major problems for in vivo MRS of this small, moving organ [6].

1.2 Potential solutions via advanced signal processing by the fast Padé transform

Clinical scanners use the fast Fourier transform (FFT) to convert the encoded time signal into its spectral representation in the frequency domain. The FFT is a low-resolution spectral estimator and can give only a total shape spectrum (envelope). A shape spectrum in the FFT is obtained from pre-assigned frequencies whose minimal separation is determined by the acquisition time, T. Attempts to improve resolution lead to a worsening of SNR [7]. The linearity of the FFT and lack of extrapolation capabilities further contribute to poor SNR. As a non-parametric estimator, the FFT requires post-processing via fitting which is non-unique. This standard procedure (FFT + fitting), can, in fact, only yield guessed estimates of the true metabolite concentrations [8].

Among the advanced signal processing methods, the fast Padé transform (FPT) is especially suitable for both in vitro and in vivo MRS [6–8]. A spectrum in the FPT, as a non-linear response function via the unique ratio of 2 polynomials, P_K / Q_K, of degree K, does not use the fixed Fourier mesh $2\pi k/T (k = 0, 1, 2, \ldots)$, and can be computed at any frequency ω. Consequently, resolution is not pre-determined by T. The conundrum between increasing T for improved resolution and increasing noise is thus averted. In contrast to the FFT, which is limited by a sharp cut-off of the time signal at the end of the acquisition time, the FPT uses its polynomial quotient to extrapolate beyond T. This feature of the FPT also contributes to improved resolution [6–8]. Being non-linear, the FPT effectively suppresses noise and thus improves SNR. Crucially, the FPT is a stable parametric signal processor, which unambiguously determines the number of true metabolites and their spectral parameters from which metabolite concentrations can be reliably reconstructed [6–8].

After the spectral parameters, namely the fundamental frequencies and the associated amplitudes $\{\omega_k, d_k\}$ $(1 \leq k \leq K)$ of the specified time signal $\{c_n\}$ $(0 \leq n \leq N-1)$ with length N and sampling time $\tau = T/N$ have been reconstructed, the FPT can automatically generate the corresponding complex-valued total shape spectrum via the rational response function in the form of the Heaviside partial fraction decomposition:

$$c_n = \sum_{k=1}^{K} d_k z_k^n \quad \Rightarrow \quad \frac{P_{K-1}(z^{-1})}{Q_K(z^{-1})} = \sum_{k=1}^{K} \frac{d_k}{z^{-1} - z_k^{-1}}. \tag{1}$$

Here, we have $z = \mathrm{e}^{i\tau\omega}$, $z_k = \mathrm{e}^{i\tau\omega_k}$, $\mathrm{Im}(\omega_k) > 0$, $\omega = 2\pi\nu$, $\omega_k = 2\pi\nu_k$ where ω and ν are the angular and linear frequency, respectively. In Eq. (1), the spectrum $\sum_{k=1}^{K} d_k/(z^{-1} - z_k^{-1})$ is summed up explicitly to yield the polynomial quotient P_{K-1}/Q_K. This is the para-diagonal Padé approximant [8]. Note that diagonal Padé approximant, P_K/Q_K is often used, as we shall do in Sect. 3.

In theoretical physics, including quantum mechanics, the Padé approximant, or the fast Padé transform as it is termed in the area of signal processing [8], has been the "work-horse". The FPT is particularly well suited for handling time signals, also called free induction decay (FID) curves, as encountered in MRS. Since there exists a time-frequency duality, the inverse fast Padé transform (IFPT) computed from Eq. (1) will give the $\{c_n\}$ as a sum of K damped complex exponentials $\{z_k\} = \{\exp(i\tau\omega_k)\}$. Analogous to the inverse FFT, the capability of the IFPT to retrieve the physical input time signal regardless of the level of noise corruption [6], is the feature which supports the use of the term "transform" in the FPT. This capability can be observed by putting the Padé spectrum from Eq. (1) into its equivalent form of continued fractions (CF) [8]. In other words, each signal point $\{c_n\}(1 \leq n \leq N-1)$ can be exactly reconstructed for any level of noise from the general analytical expression for the expansion coefficients $\{a_n\}$ in the CF [8]. Thus, the optimal mathematical model for the frequency spectrum of these FIDs is prescribed quantum-mechanically as the finite-rank response Green function in the form of the unique ratio of two polynomials, namely the fast Padé transform. Just as in the time domain, for which the Schrödinger time evolution operator predicts the FID as the sum of damped exponentials, the same quantum physics determines that the frequency spectrum is provided by the Green function via the Padé quotient of two polynomials from Eq. (1). It is for this reason that the FPT has shown such an unprecedented algorithmic success in yielding exact reconstructions [6,8].

There are two complementary versions of the fast Padé transform: the FPT$^{(+)}$ and FPT$^{(-)}$. In the diagonal form, these have the following representations for the exact infinite-rank Green function, which is defined as the Maclaurin series with the time signal points $\{c_n\}$ as the expansion coefficients:

$$G(z^{-1}) \equiv \sum_{n=0}^{\infty} c_n z^{-n-1} \qquad ; \quad \text{Exact}, \tag{2}$$

$$G(z^{-1}) \approx G_K^{(+)}(z) \equiv \frac{P_K^+(z)}{Q_K^+(z)} = \frac{\sum_{r=1}^{K} p_r^+ z^r}{\sum_{s=0}^{K} q_r^+ z^s} \qquad ; \quad \text{FPT}^{(+)}, \tag{3}$$

$$G(z^{-1}) \approx G_K^{(-)}(z^{-1}) \equiv \frac{P_K^-(z^{-1})}{Q_K^-(z^{-1})} = \frac{\sum_{r=0}^{K} p_r^- z^{-r}}{\sum_{s=0}^{K} q_r^- z^{-s}}; \quad \text{FPT}^{(-)}. \tag{4}$$

We can exactly and uniquely extract the expansion coefficients $\{p_r^{\pm}, q_s^{\pm}\}$ of the numerator $P_K^{\pm}(z^{\pm 1})$ and denominator $Q_K^{\pm}(z^{\pm 1})$ polynomials from the time signal points $\{c_n\}$ by solving a single system of linear equations from definitions (3) and (4), after truncation of the Maclaurin series for $G(z^{-1})$ at $n = N - 1$.

An equivalent way of expressing the spectra $P_K^{\pm}(z^{\pm 1})/Q_K^{\pm}(z^{\pm 1})$ is through the canonical forms:

$$\frac{P_K^{\pm}(z^{\pm 1})}{Q_K^{\pm}(z^{\pm 1})} = \frac{p_K^{\pm}}{q_K^{\pm}} \prod_{k=1}^{K} \frac{z^{\pm 1} - z_{k,P}^{\pm}}{z^{\pm 1} - z_{k,Q}^{\pm}}. \tag{5}$$

The roots of the characteristic equations, $Q_K^{\pm}(z^{\pm 1}) = 0$ have the solutions $z_k^{\pm 1} \equiv z_{k,Q}^{\pm 1} (1 \le k \le K)$. These are a constituent part of the fundamental harmonics via $\{d_k^{\pm}, z_{k,Q}^{\pm 1}\}$. The associated fundamental amplitudes $d_k^{\pm}$are the Cauchy residues of the spectra from Eq. (5). Thus, when the roots are non-degenerate, $(z_{k',Q}^{\pm 1} \ne z_{k,Q}^{\pm 1}, k' \ne k)$, these amplitudes are defined by:

$$d_k^{\pm} = \lim_{z^{\pm 1} \to z_{k,Q}^{\pm}} \left\{ \left(z^{\pm 1} - z_{k,Q}^{\pm 1} \right) \left[P_K^{\pm}(z^{\pm}) / Q_K^{\pm}(z^{\pm}) \right] \right\}, \tag{6}$$

and thus:

$$d_k^{\pm} = \frac{P_K^{\pm}\left(z_{k,Q}^{\pm}\right)}{\left(\mathrm{d}/\mathrm{d}z_{k,Q}^{\pm}\right) Q_K^{\pm}\left(z_{k,Q}^{\pm}\right)} = \frac{p_K^{\pm}}{q_K^{\pm}} \prod_{k'=1}^{K} \frac{z_{k,Q}^{\pm} - z_{k',P}^{\pm}}{\left(z_{k,Q}^{\pm} - z_{k',Q}^{\pm}\right)_{k' \ne k}}, \tag{7}$$

$$\Rightarrow d_k^{\pm} \propto \left(z_{k,Q}^{\pm} - z_{k,P}^{\pm} \right). \tag{8}$$

Therein, $(\mathrm{d}/\mathrm{d}z_{k,Q}^{\pm}) Q_K^{\pm}(z_{k,Q}^{\pm})$ is the first derivative of the denominator polynomials. Therefore, each amplitude represents the distance between the pole and zero, $d_k^{\pm} \propto z_{k,Q}^{\pm} - z_{k,P}^{\pm}$, as per (8). Accordingly, the Cauchy residue reflects the behavior of a line integral of a meromorphic function around a specified pole. With this, the reconstruction of the $2K$ complex fundamental parameters $\{\omega_k^{\pm}, d_k^{\pm}\}$ within the $\text{FPT}^{(\pm)}$ is completed. The expressions for $G_K^{(+)}(z)$ and $G_K^{(-)}(z^{-1})$ from Eqs. (3) and (4) provide an approximation to the same Green function $G(z^{-1})$. With respect to the input Maclaurin series $G(z^{-1})$, the Green function $G_K^{(-)}(z^{-1})$ is convergent outside the unit circle ($|z| > 1$), and divergent inside the unit circle ($|z| < 1$). The convergence rate of $G_K^{(-)}(z^{-1})$ is more rapid than the original Maclaurin series, and thus the $\text{FPT}^{(-)}$ is an accelerator of convergence. In contrast, the $\text{FPT}^{(+)}$ via $G_K^{(+)}(z)$ uses the variable z. It thereby converges inside the unit circle ($|z| < 1$) which is where the exact Green function $G(z^{-1})$ diverges. The $\text{FPT}^{(+)}$ has the more difficult task of converting divergent series into convergent ones via the principle of Cauchy analytical continuation.

The key point is that the FPT$^{(+)}$ and FPT$^{(-)}$ work in a complementary manner, inside and outside the unit circle, respectively. Internal cross-validation is provided when full convergence is achieved in the FPT$^{(-)}$. In other words, $\omega_k^+ \approx \omega_k^- \equiv \omega_k$ and $d_k^+ \approx d_k^- \equiv d_k$ where $\{\omega_k, d_k\}$ are the complex frequencies and amplitudes from the FID of Eq. (1). In such a case, the FPT$^{(\pm)}$ exactly solve the harmonic inversion problem, which is called quantification in MRS. This is achieved using only the sampled time signal $\{c_n\}$ in order to reconstruct all the complex fundamental frequencies and amplitudes $\{\omega_k, d_k\}$, as per Eq. (1).

Since the poles are the only singularities, the spectra $P_K^{\pm}(z^{\pm 1})/Q_K^{\pm}(z^{\pm 1})$ are meromorphic functions. The poles $\{z_{k,Q}^{\pm}\}$ and zeros $\{z_{k,P}^{\pm}\}$ of these spectra are the roots of $Q_K^{\pm}(z^{\pm 1}) = 0$ and $P_K^{\pm}(z^{\pm 1}) = 0$, respectively. The harmonic variables $z_k^{\pm 1}$ are denoted as $z_{k,Q}^{\pm}$ and $z_{k,P}^{\pm}$ by adding the subscripts P and Q to refer to the numerator $P_K^{\pm}(z^{\pm 1})$ and denominator $Q_K^{\pm}(z^{\pm 1})$ polynomials. The spectral poles and zeros yield the physical parameters of the system which generated the FIDs as a response to an external excitation. The amplitudes, i.e. the intensities of the FID, are likewise directly related to the spectral poles and zeros since $d_k^{\pm} \propto z_{k,Q}^{\pm} - z_{k,P}^{\pm}$, according to Eq. (8). Actually, the FPT$^{(\pm)}$ links the two separate representations called the poles of the FPT$^{(\pm)}$ and the zeros of the FPT$^{(\pm)}$, as denoted by pFPT$^{(\pm)}$ and zFPT$^{(\pm)}$, respectively.

Poles that are stable against external perturbations are genuine or physical. On the other hand, when exposed to even the slightest perturbation, unstable poles oscillate widely. These unstable poles do not ever converge with increased degree of the Padé polynomial. In other words, the latter are similar to the behavior of noise or noise-like corruption, i.e. they act as random fluctuations.

By examining the spectral poles and zeros in the FPT$^{(\pm)}$, stable and unstable poles can be clearly distinguished. In the case of the stable structures, the poles and zeros are distinct, i.e. they do not coincide, $z_{k,Q}^{\pm} \neq z_{k,P}^{\pm}$. By contrast, the unstable structures show confluence of poles and zeros, namely $z_{k,Q}^{\pm} \approx z_{k,P}^{\pm}$, and these coincident or nearly coincident poles and zeros are termed Froissart doublets. Since $d_k^{\pm} \propto z_{k,Q}^{\pm} - z_{k,P}^{\pm}$ according to Eq. (8), genuine resonances ($z_{k,Q}^{\pm} \neq z_{k,P}^{\pm}$) have nonzero amplitudes. On the other hand, spurious resonances ($z_{k,Q}^{\pm} = z_{k,P}^{\pm}$ or $z_{k,Q}^{\pm} \approx z_{k,P}^{\pm}$) have zero or nearly zero amplitudes and, for that reason, they are extremely unstable when exposed to even minimal perturbation. Adding even the smallest amount of random Gaussian noise to an FID could noticeably alter the distribution of spurious frequencies and amplitudes in the complex plane. Consequently, if K in $P_K^{\pm}/Q_K^{\pm}$ has stabilized so that all the genuine resonances have been identified, continuing to compute the Padé spectra for a higher degree polynomial, $K+m$ ($m = 1, 2, 3, \ldots$), would only yield new spurious resonances for a positive integer m. This would automatically imply that $z_{k,Q}^{\pm} = z_{k,P}^{\pm}$ and, hence, $d_k^{\pm} = 0$ for $k = K + m$ ($m = 1, 2, 3, \ldots$). All the numerator and denominator terms with spurious poles ($z^{\pm 1} - z_{k,Q}^{\pm}$) and spurious zeros ($z^{\pm 1} - z_{k,P}^{\pm}$) in the canonical forms from Eq. (5) would cancel. As a consequence, pole-zero cancellation occurs, with stabilization of the computed spectra:

$$\frac{P^{\pm}_{K+m}(z^{\pm 1})}{Q^{\pm}_{K+m}(z^{\pm 1})} = \frac{P^{\pm}_{K}(z^{\pm 1})}{Q^{\pm}_{K}(z^{\pm 1})} \quad (m = 1, 2, 3, \ldots). \tag{9}$$

From the above presentation, it follows that Padé reconstruction actually treats the number of genuine resonances, i.e. the number of fundamental harmonics K as an unknown parameter. With convergence of the reconstructed frequencies and amplitudes, the parameter K is determined. In practice, this is achieved by gradually increasing the degree of the Padé polynomials until the genuine frequencies and amplitudes stabilize. Any further increase in the polynomial degree yields only spurious resonances that are readily detected because of their instability and pole-zero confluences that yield zero or near-zero amplitudes. This is termed "Signal-Noise Separation" (SNS), and has been established within MRS for both noiseless and noise-corrupted MR time signals [9, 10].

1.3 Progress to date using the FPT for MRS data from the ovary and aim of the present study

In our recent comparative study, the resolution performance of the FPT was found to be far superior to the FFT, when applied to noiseless time signals that were generated according to in vitro MRS data as encoded from malignant and benign ovarian cyst fluid [11,12]. The associated encoded data were from [13]. We also demonstrated the capability of the FPT to reconstruct the spectral parameters from this noiseless MRS data for malignant and benign ovarian cyst fluid. Thereby, we could unequivocally deduce the metabolite concentrations, which are the clinically most relevant MRS data for distinguishing cancerous from benign ovarian lesions.

In the present paper, we add random Gauss-distributed zero mean noise, in order to examine the resolution performance of the FPT in a more realistic, yet fully controlled setting. This is a key preparatory step for application to MR time signals encoded in vivo and in vitro from ovarian cancer and benign ovarian lesions. Such a systematic validation of the fast Padé transform has already been accomplished with the corresponding FIDs from brain MRS data [6,14].

2 Data analysis

We applied the FPT$^{(-)}$ to a synthesized time signal reminiscent of in vitro MRS data as encoded from malignant ovarian cyst fluid [13]. The procedure was as follows. The input data for the spectral parameters $\{K, \omega_k, d_k\}$ were derived from those reported for median concentrations C_{met} (expressed in μM/L ww, where ww stands for wet weight) of twelve metabolites for cancerous ovarian cyst fluid obtained from twelve patients, as reported in [13].

The input peak amplitudes were extracted from the data in [13] using the quotient $2C_{met}/C_{ref}$. The reference concentration C_{ref} was taken as the largest concentration (6536 μM/L ww) [lactate] from the malignant cyst fluid. The phases φ_k $(1 \leq k \leq 12)$

Table 1 Input data based upon in vitro MRS data as encoded from malignant ovarian cyst fluid [13]

n_k^o (metabolite #k)	Re(ν_κ) (ppm)	Im(ν_k) (ppm)	$\lvert d_k \rvert$ (au)	C_k (μM/L ww)	M_k (assignment)
Input data: spectral parameters, concentrations and metabolite assignments					
1	1.023	0.0008	0.024	78	Isoleucine (Iso)
2	1.042	0.0008	0.121	395	Valine (Val)
3	1.331	0.0008	0.076	248	Threonine (Thr)
4	1.412	0.0008	2.000	6536	Lactate (Lac)
5	1.513	0.0008	0.179	585	Alanine (Ala)
6	1.721	0.0008	0.150	490	Lysine (Lys)
7	2.132	0.0008	0.019	62	Methionine (Met)
8	2.473	0.0008	0.253	827	Glutamine (Gln)
9	3.052	0.0008	0.020	65	Creatine (Cr)
10	3.131	0.0008	0.024	78	Creatinine (Crn)
11	3.192	0.0008	0.013	42	Choline (Cho)
12	5.223	0.0008	0.080	261	Glucose (Glc)

Hereafter, Re(ν_k) denotes chemical shift in dimensionless units of parts per million (ppm), peaks widths [Im(ν_k)] are also in ppm, peak heights are in au (arbitrary units), and metabolite concentrations are in micro-mole per liter (μM/L ww), where ww denotes wet weight. The abbreviations for the metabolites given herein are used in the subsequent table and figures

from the complex amplitudes d_k were all set to zero, so that every amplitude d_k is real, $d_k = |d_k|$. The line-widths [related to Im(ω_k)] in [13] were estimated to be approximately 1 Hz. The chemical shifts [Re(ω_k)], as the positions of the fundamental resonances (peaks) for the twelve metabolites are taken from [13]. The input data for peak positions, line widths, peak heights and concentrations of the twelve metabolites for malignant ovarian fluid are listed in Table 1.

A magnetic resonance (MR) time signal corresponding to malignant ovarian cyst fluid was then generated. This time signal $\{c_n\}$ was sampled from the sums of twelve complex damped harmonics, $c_n = \sum_{k=1}^{K} d_k e^{in\tau\omega_k} (0 \le n \le N-1)$ where N is the total signal length. Here, the d_k's are the stationary amplitudes and τ is the sampling time ($\tau = T/N$). Further, the ω_k's are the complex angular fundamental frequencies with Im(ω_k) > 0 ($1 \le k \le K$), where K is the total number of harmonics, which is set to $K = 12$, according to [13].

The time signals from [13] were recorded using a static magnetic field strength $B_0 \approx 14.1$ T (Larmor frequency of 600 MHz) and a bandwidth of 6667 Hz. We used the inverse of this bandwidth for the sampling time τ. The total signal length N was selected in [13] to satisfy the Fourier resolving power $\Delta\omega_{\min} = 2\pi/T$. This would yield a spectral resolution $\Delta\omega = 0.02$ parts per million (ppm), which should split apart isoleucine and valine, the two most tightly spaced metabolites. To this end, the closest integer in the composite form 2^m for the time signal length required by the FFT is $N = 2^{15} = 32768$. Since, as mentioned, the FPT resolution is not predetermined by $2\pi/T$, a much shorter time signal length could suffice, we sampled our time signals using only $N = 1024$.

To create the noisy FID, Gauss-distributed zero mean noise was added with a standard deviation $\sigma = 0.01156$ multiplying the root-mean-square (RMS) of the noiseless time signal. The number 0.01156 is nearly the height of the smallest peak in the spectrum (choline, peak #11 at 3.192 ppm). This noise level is considered quite realistic for encoded data.

Once the spectral parameters $\{K, \omega_k, d_k\}(1 \leq k \leq K, K = 12)$ were fixed, together with N and τ, the signals $\{c_n\}$ could be sampled from the sum of 12 attenuated complex exponentials $\{\exp(i\tau n\omega_k)\}$. When such sampled sets $\{c_n\}$ became available, they were treated as if K and $\{\omega_k, d_k\}$ were completely unknown. As such, the task of quantification was to reconstruct K as well as $\{\omega_k, d_k\}$ $(1 \leq k \leq K)$ using only the given N, τ and the digitized data $\{c_n\}$ $(0 \leq n \leq N-1)$, as would also be done with the corresponding encoded FID. Thus, both experimentally measured and theoretically generated time signals can be quantified in the same manner, using the same spectral analysis. Presently, we shall accomplish this task by applying the FPT$^{(-)}$ variant to the simulated noiseless and noisy time signals to set the standard. The theory and algorithms of the fast Padé transform are given in [6–10,14].

3 Results

On the left half of Table 2, the peak positions, line widths, peak heights and computed metabolite concentrations are shown for malignant ovarian cyst data as reconstructed by the FPT$^{(-)}$, without added noise. These reconstructed data are presented for three signal lengths, $N/32 = 32$, $N/16 = 64$ and $N/8 = 128$. For the noiseless case, with 32 signal points, nine of the twelve peaks were identified, whereas isoleucine at 1.023 ppm (peak #1), threonine at 1.331 ppm (peak #3) and choline at 3.192 ppm (peak #11) were missing. Thus, 32 time signal points were insufficient to converge to all the physical resonances. However, with $N/16 = 64$ signal points, the FPT *exactly* reconstructed all the spectral parameters of each of the twelve peaks for the malignant ovarian data [panel (ii)]. It can be seen that at the signal length $N/16 = 64$ all the Padé-reconstructed parameters are identical to the input data and that the retrieved metabolite concentrations are exactly equal to the input concentrations from Table 1. The obtained convergence is stable at longer partial signal lengths, as seen by comparing panels (ii) and (iii), with the latter being at signal length of $N/8 = 128$, since all the reconstructed data for $N/16$ and $N/8$ are identical with the input data. We have also presently confirmed stability at even longer partial signal lengths as well as for half $(N/2 = 512)$ and the full signal length $(N = 1024)$ for all the genuine peak parameters reconstructed by the FPT$^{(-)}$.

On the right half of Table 2, the peak positions, linewidths, heights and computed concentrations are shown for malignant ovarian cyst data as reconstructed by the FPT$^{(-)}$, with added noise. These reconstructed data are presented for the same three signal lengths, $N/32 = 32$, $N/16 = 64$ and $N/8 = 128$. As in the noiseless case, with 32 signal points, nine of the twelve peaks were identified; isoleucine at 1.023 ppm, threonine at 1.331 ppm and choline at 3.192 ppm were missing. At $N/16 = 64$ signal points, all twelve resonances were identified, but many of the signal parameters were incorrect. Notably, the computed concentration of isoleucine was much lower than its

Table 2 Padé-reconstruction of spectral parameters and metabolite concentrations based upon in vitro MRS data as encoded from malignant ovarian cyst fluid [13] for the noiseless case (*left* column) and in the presence of level 0.01156 RMS (root mean square) added noise (*right* column)

n_k^o (#k)	$\mathrm{Re}(\nu_k^-)$ (ppm)	$\mathrm{Im}(\nu_k^-)$ (ppm)	$\lvert d_k^- \rvert$ (au)	C_k^- (μM/L ww)	M_k	n_k^o (#k)	$\mathrm{Re}(\nu_k^-)$ (ppm)	$\mathrm{Im}(\nu_k^-)$ (ppm)	$\lvert d_k^- \rvert$ (au)	C_k^- (μM/L ww)	M_k
Convergence of spectral parameters and concentrations (malignant) in $\mathrm{FPT}^{(-)}$; FID length: N/M, $N=1{,}024$, $M=8$–32											
(i) N/32 = 32 (noiseless)						*(iv) N/32 = 32 (noisy)*					
2	1.041	0.0015	0.148	484	Val	2	1.042	0.0018	0.145	474	Val
4	1.411	0.0013	2.050	6699	Lac	4	1.412	0.0013	2.103	6873	Lac
5	1.450	0.0083	0.196	641	Ala	5	1.545	0.0941	0.304	993	Ala
6	1.713	0.0039	0.174	572	Lys	6	1.737	0.0353	0.086	281	Lys
7	2.105	0.0300	0.029	92	Met	7	2.000	0.9024	0.061	199	Met
8	2.473	0.0008	0.252	824	Gln	8	2.473	0.0010	0.248	810	Gln
9	3.073	0.0029	0.029	95	Cr	9	3.083	0.0412	0.037	121	Cr
10	3.168	0.0034	0.028	92	Crn	10	3.159	0.0309	0.038	124	Crn
12	5.223	0.0008	0.080	261	Glc	12	5.223	0.0008	0.080	261	Glc
(ii) N/16 = 64 (noiseless): converged						*(v) N/16 = 64 (noisy)*					
1	1.023	0.0008	0.024	78	Iso	1	0.946	0.0797	0.004	13	Iso
2	1.042	0.0008	0.121	395	Val	2	1.041	0.0015	0.147	480	Val
3	1.331	0.0008	0.076	248	Thr	3	1.318	0.0166	0.082	268	Thr
4	1.412	0.0008	2.000	6536	Lac	4	1.412	0.0009	1.993	6513	Lac
5	1.513	0.0008	0.179	585	Ala	5	1.511	0.0028	0.184	601	Ala
6	1.721	0.0008	0.150	490	Lys	6	1.721	0.0009	0.150	490	Lys
7	2.132	0.0008	0.019	62	Met	7	2.132	0.0010	0.019	62	Met
8	2.473	0.0008	0.253	827	Gln	8	2.473	0.0008	0.253	827	Gln
9	3.052	0.0008	0.020	65	Cr	9	3.053	0.0017	0.021	69	Cr
10	3.131	0.0008	0.024	78	Crn	10	3.133	0.0029	0.023	75	Crn
11	3.192	0.0008	0.013	42	Cho	11	3.195	0.0032	0.013	42	Cho
12	5.223	0.0008	0.080	261	Glc	12	5.223	0.0008	0.080	261	Glc

Table 2 continued

n_k^o (#k)	Re(ν_k^-) (ppm)	Im(ν_k^-) (ppm)	$\lvert d_k^- \rvert$ (au)	C_k^- (μM/L ww)	M_k	n_k^o (#k)	Re(ν_k^-) (ppm)	Im(ν_k^-) (ppm)	$\lvert d_k^- \rvert$ (au)	C_k^- (μM/L ww)	M_k
(iii) N/8 = 128 (noiseless): converged						*(vi) N/8 = 128 (noisy): converged*					
1	1.023	0.0008	0.024	78	Iso	1	1.023	0.0008	0.024	78	Iso
2	1.042	0.0008	0.121	395	Val	2	1.042	0.0008	0.121	395	Val
3	1.331	0.0008	0.076	248	Thr	3	1.331	0.0008	0.076	248	Thr
4	1.412	0.0008	2.000	6536	Lac	4	1.412	0.0008	2.000	6536	Lac
5	1.513	0.0008	0.179	585	Ala	5	1.513	0.0008	0.179	585	Ala
6	1.721	0.0008	0.150	490	Lys	6	1.721	0.0008	0.150	490	Lys
7	2.132	0.0008	0.019	62	Met	7	2.132	0.0008	0.019	62	Met
8	2.473	0.0008	0.253	827	Gln	8	2.473	0.0008	0.253	827	Gln
9	3.052	0.0008	0.020	65	Cr	9	3.052	0.0008	0.020	65	Cr
10	3.131	0.0008	0.024	78	Crn	10	3.131	0.0008	0.024	78	Crn
11	3.192	0.0008	0.013	42	Cho	11	3.192	0.0008	0.013	42	Cho
12	5.223	0.0008	0.080	261	Glc	12	5.223	0.0008	0.080	261	Glc

In the noiseless case, the Padé-reconstructed data are converged at partial signal length, $N/16 = 64$, where $N = 1024$ [panel (ii)]. With added background noise, the reconstructed data are converged at partial signal length, $N/8 = 128$ [panel (vi)]

actual value (13 μM/L ww rather than 78 μM/L ww). However, at $N/8 = 128$ signal points for the noisy FID, the FPT$^{(-)}$ reconstructed all the spectral parameters and the computed metabolite concentrations were all correct.

The convergence of metabolite concentrations for the noiseless (left panels) and noisy cases (right panels) are graphically illustrated in Fig. 1 for the three partial signal lengths: $N/32 = 32$, $N/16 = 64$ and $N/8 = 128$. The input data are represented by the symbol "x", whereas the Padé-reconstructed data are shown as open circles. For the noiseless case, prior to convergence, at $N/32 = 32$ only the concentration of glucose is correctly assessed [top left panel (i)]. At $N/16 = 64$ [left middle panel (ii)] and $N/8 = 128$ [left bottom panel (iii)], all of the metabolite concentrations are correct, as seen both numerically and by the graphic representations. This means that the "x's" are completely centered within the open circles, indicating full agreement between the input and reconstructed data for the noiseless FID. Similarly, for the noisy case at $N/3 = 32$ only the concentration of glucose is correctly assessed [top right panel (iv)]. However, at $N/16 = 64$ [right middle panel (v)], the computed concentrations were fully correct only for lysine, methionine, glutamine, choline and glucose. At $N/8 = 128$ [right bottom panel (vi)], all of the metabolite concentrations are correct, as seen both numerically and by the graphic representations.

Since for the noisy case, convergence was achieved at 128 signal points, altogether 64 resonances were reconstructed. Of these, 52 resonances were spurious and 12 were genuine. Within the illustrative frequency window from 1.6 to 6 ppm, containing 7 genuine resonances, after convergence has been reached, the concept of Froissart doublets for the noiseless and noisy data is demonstrated in Fig. 2. Panels (i) and (ii) display the Argand plots [$\mathrm{Re}(\nu_k^-)$ vs. $\mathrm{Im}(\nu_k^-)$, where ν_k^- is the linear frequency, $\omega_k^- = 2\pi\nu_k^-$] for the genuine and spurious resonances. Panels (i) and (ii) show that all the spurious resonances are Froissart doublets, namely that the poles, marked as open circles, coincide with the corresponding zeros, denoted by small filled circles (dots). This is a graphic representation of pole-zero confluence. In panel (i) depicting the noiseless case, these Froissart doublets show a rather regular alignment along the ordinate within the major portion (∼3.5–6 ppm) of the displayed part of the whole Nyquist interval. Interspersed with the Froissart doublets, there are seven genuine resonances, indicated by the coincidence between the input poles (x's) and the Padé-reconstructed poles. Panel (ii) of Fig. 1 displays the noisy case, which differs from the noiseless case only in that the Froissart doublets show a more irregular distribution along the entire ordinate for the shown frequency window. In the bottom panel (iii) of Fig. 1, it can be seen that all the spurious resonances have zero amplitudes, whereas the absolute values of the amplitudes of the seven genuine reconstructed resonances all have non-zero values.

Figure 3 shows the convergence of the absorption total shape spectra at three signal lengths for the Padé-reconstructed malignant ovarian cyst data. The left three panels display the absorption spectra generated by the FPT$^{(-)}$ at $N/32 = 32$ [top (i)], $N/16 = 64$ [middle (ii)] and $N/8 = 128$ [bottom (iii)], for the noiseless case. On the top left panel (i), nine of the twelve peaks are seen. More signal points are needed for the appearance of the other three resonances: isoleucine, threonine and the second resonance in the region between 3.1 and 3.2 ppm. At $N/16 = 64$ signal length, these latter three peaks are resolved and the heights of all twelve peaks are correct [middle left panel (ii)]. Again, consistent with Table 2, at $N/16 = 64$ the absorption spectrum

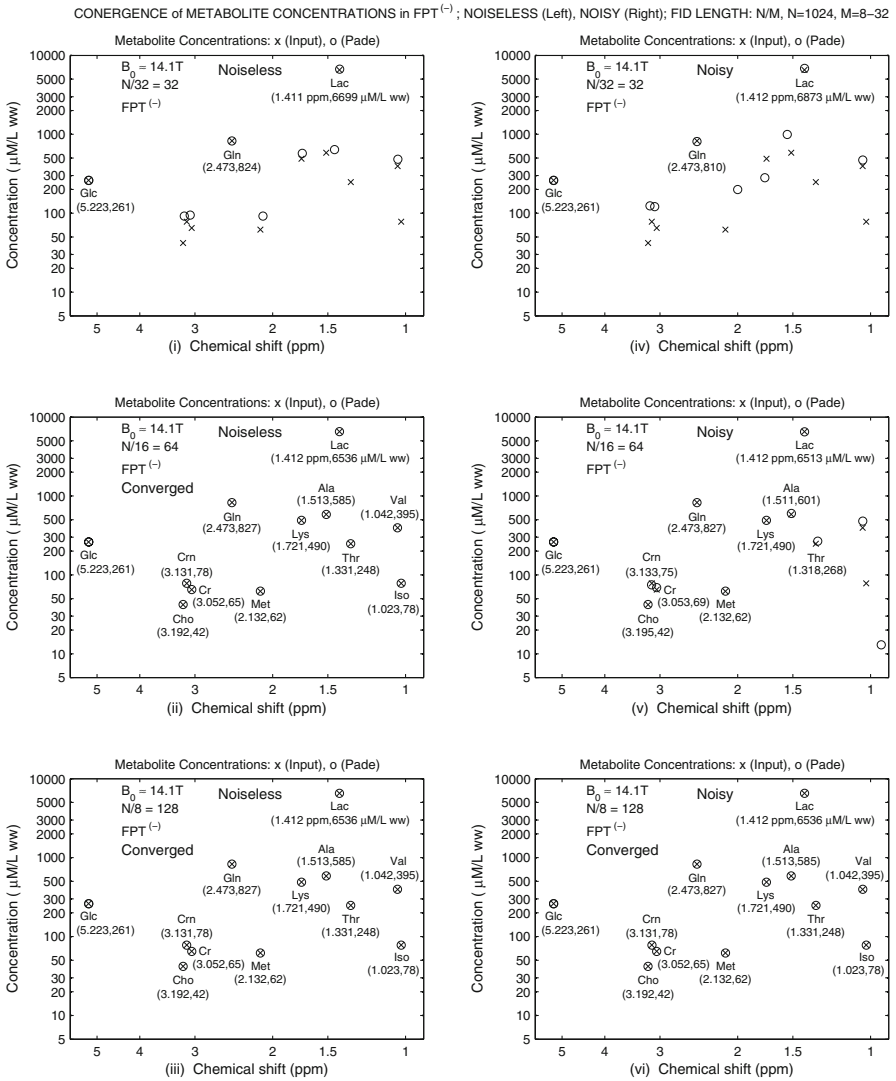

Fig. 1 Metabolite concentrations based upon Padé-reconstruction for the noiseless (*left panels*) and noisy case (*right panels*) for malignant ovarian cyst data from [13]. Three partial signal lengths: $N/32 = 32$, $N/16 = 64$ and $N/8 = 128$, are shown for both cases. Convergence is achieved at $N/16 = 64$ signal points for the noiseless case [*panel (ii)*]. For the noisy case, $N/8 = 128$ signal points are needed for convergence [*panel (vi)*]

is fully converged in the FPT$^{(-)}$ for the noiseless case and is stable at $N/8 = 128$ [bottom (iii)]. The right three panels display the absorption total shape spectra of the FPT at $N/32 = 32$ [top (iv)], $N/16 = 64$ [middle (v)] and $N/8 = 128$ [bottom (vi)], for the noisy case. On the top right panel (iv), only four of the twelve peaks are clearly identified with approximately the correct heights; these are valine, lactate, glutamine and glucose. At $N/16 = 64$ signal length, eleven of the twelve peaks are detected.

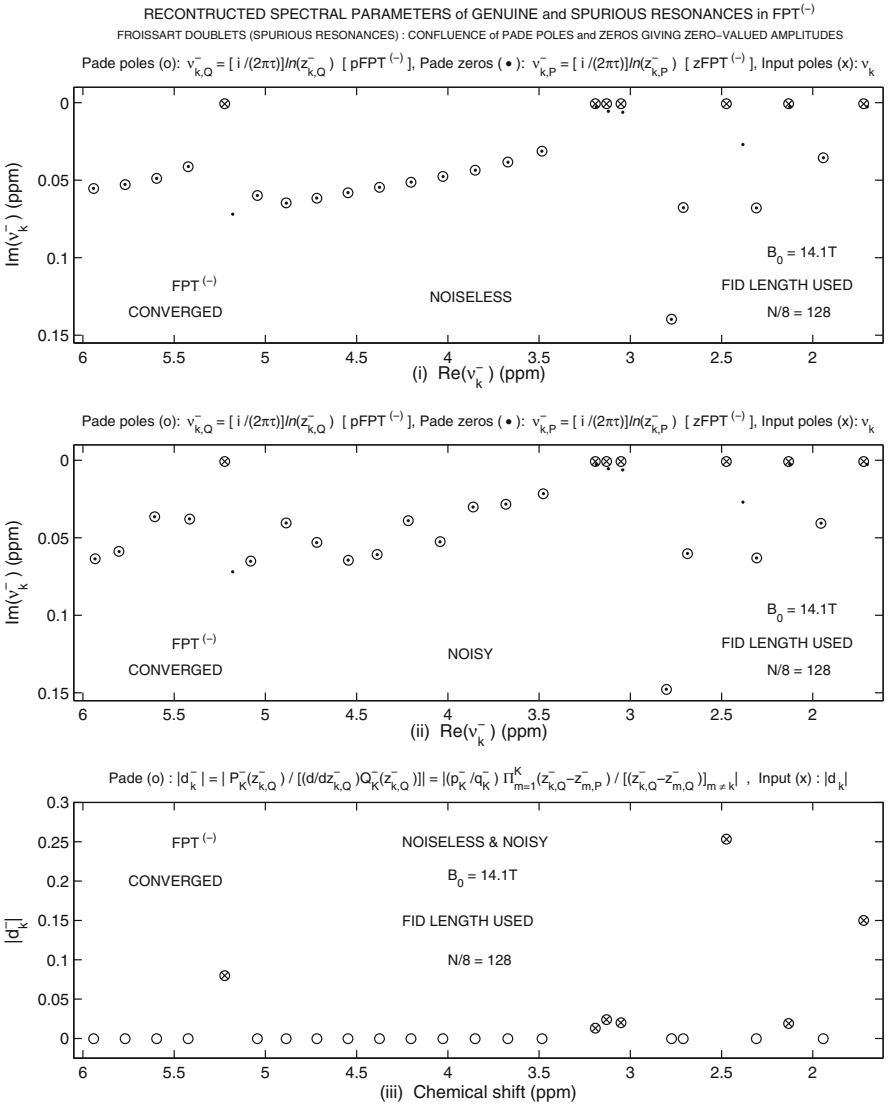

Fig. 2 Use of Froissart doublets to distinguish the genuine from the spurious frequencies and amplitudes of the spectral parameters reconstructed by the $\text{FPT}^{(-)}$ within the frequency window between 1.6 and 6 ppm, based upon malignant ovarian cyst data from [13]. Argand plots for the noise free signal [*top panel (i)*] and for the noise-corrupted time signal [*middle panel (ii)*]. All the spurious (Froissart) amplitudes in both the noiseless and noisy cases are also identified by their zero values [*bottom panel (iii)*]

Isoleucine cannot yet be seen on the total shape spectrum. The peak heights are low for choline, creatinine and creatine in the region between ∼3.0 and 3.2 ppm, as well as for alanine at ∼1.5 ppm. The peak height of threonine at ∼1.33 ppm is very low and peak broadening occurs. Again, coherent with Table 2, $N/8 = 128$ [bottom (vi)], the absorption total shape spectrum is fully converged for the noisy case. The absorption

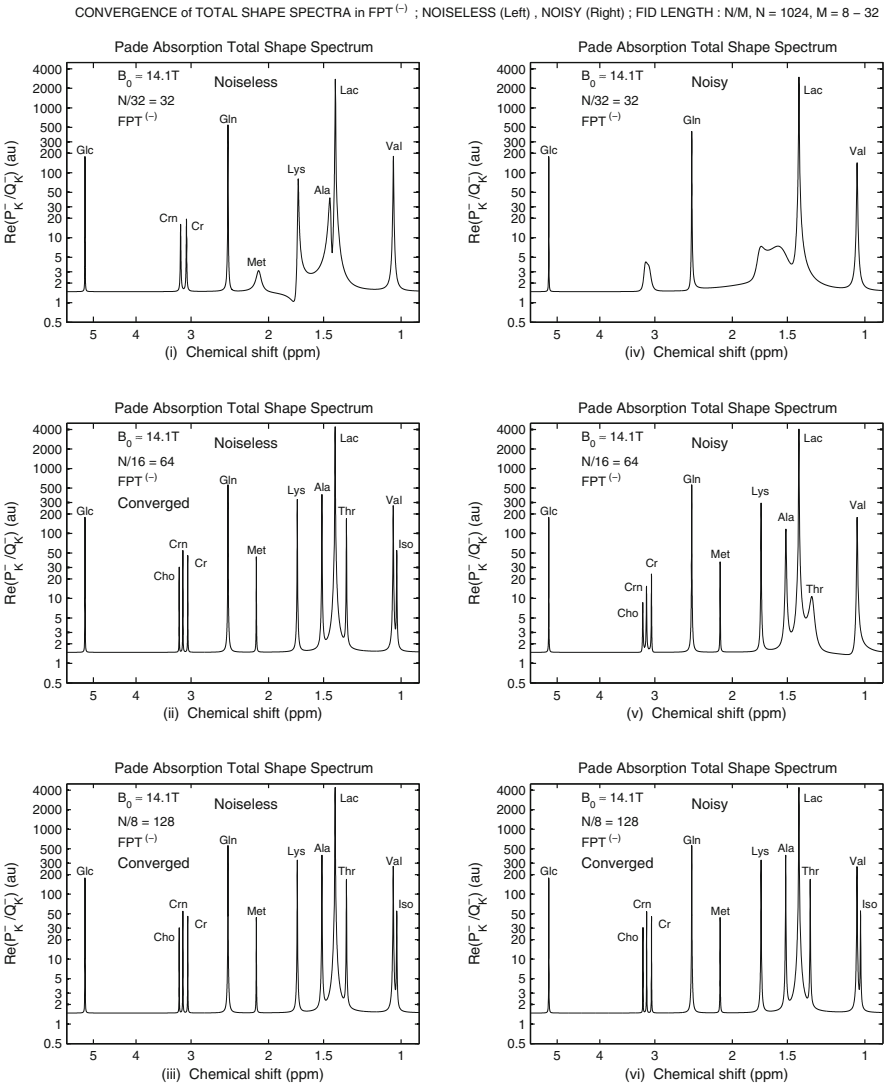

Fig. 3 Comparison of the resolution performance of the FPT$^{(-)}$ for noiseless [*left panels (i), (ii)* and *(iii)*] and noisy [*right panels (iv) (v)* and *(vi)*] total absorption shape spectra of malignant ovarian cyst data from [13] at three short partial signal lengths. At $N/32 = 32$ signal points (*top left panel (i)* without noise the FPT$^{(-)}$ has resolved 9 of the 12 peaks. At $N/16 = 64$ signal length, these latter three peaks are resolved, the heights of all twelve peaks are correct [*middle left panel (ii)*], and the total absorption shape spectrum is fully converged. This convergence is stable at $N/8 = 128$ [*bottom* (iii)], for the noiseless case. On the *top right panel (iv)* for the noisy case at $N/32 = 32$, only four of the twelve metabolites are clearly detected with approximately correct heights. At $N/16 = 64$ signal length, eleven of the twelve peaks are clearly identified, but the peak heights are low for several of the peaks [*right middle panel (v)*]. At $N/8 = 128$ [*bottom panel (vi)*], the absorption spectrum is fully converged for the noisy case

total shape spectra remained converged at longer fractions $N/M (M < 4)$ of the full time signal including $N = 1024$, such that the spectra reconstructed by the FPT$^{(-)}$ stayed unchanged for both the noiseless and noisy cases. This effectively amounts to both noise suppression and dimensionality reduction by the fast Padé transform. These two features are responsible for the achieved exact reconstruction, even for noisy time signals.

4 Discussion

Applied to these MRS data from malignant ovary and in the presence of realistic background noise, the resolution performance of the fast Padé transform is striking. With only 128 data points out of 1024 sampled, the Padé-reconstructed total absorption shape spectra were fully converged. The intensity of MR time signals is the highest early in the encoding, but subsequently it decays exponentially. It is thus desirable to encode the time signal as quickly as possible in order to avoid long acquisition times when mainly noise will be generated, especially for clinical signals that are encoded at lower magnetic field strengths. It is indeed likely that reliance upon Fourier-based signal processing has been the major reason for the poor resolution when in vivo MRS is applied to the ovary. Our previous comparison between the performance of the FFT and the FPT on noiseless MRS data from the ovary revealed that convergence was achieved at 512 times shorter signals in the FPT. Specifically, convergence of the total absorption shape spectra using the FFT required 32768 signal points, compared to 64 signal points with the FPT [12]. Since the FFT showed such poor results in our previous study on noiseless MRS data from the ovary [12], further comparisons between Fourier and Padé processing of ovarian MRS data in the presence of noise would be entirely superfluous, and, as such, is left out.

Rather, the salient question for the present paper is how well does the FPT perform in the important practical setting of quantifying noise-corrupted MRS time signals? Beginning with a consideration of the total absorption shape spectra, in the presence of realistic background noise, the FPT$^{(-)}$ requires twice more signal points to converge, compared to its performance on noiseless signals. Notably, prior to convergence at $N/16 = 64$ signal points, isoleucine which resonates at 1.023 ppm, was not detected on the total absorption shape spectrum. Instead, the closely-lying valine peak at 1.042 ppm appeared to be somewhat widened and asymmetric. This observation could be of clinical relevance since isoleucine and valine that are observed in the interval between 1.02 and 1.04 ppm reportedly show significant differences in non-cancerous and malignant ovarian cyst fluid [13]. In the latter, higher concentrations of these branched-chain amino acids are interpreted as being protein breakdown products from necrosis and proteolysis. Taken together, these considerations underscore the vital importance of ensuring that the total absorption shape spectra are fully converged. We have elsewhere given examples in which close-to but still prior-to convergence, information inferred from the total absorption shape spectrum may be incorrect. This includes metabolite ratios, upon which much clinical decision-making is based in oncology and elsewhere [15].

Whereas convergence of the total shape spectrum is necessary, it is clearly insufficient to guarantee that the spectral structures have been identified, let alone accurately quantified. The latter requires stable parametric processing, with unequivocal distinction between genuine and spurious spectral information. For the present problem of ovarian cancer MRS data, there were over four times more non-physical than true resonances when convergence of all the spectral parameters was achieved. It was clearly demonstrated that these spurious resonances were characterized by pole-zero cancellation with regard to the complex frequencies and by the corresponding zero-valued amplitudes. It should be pointed out that the number of spurious resonances and their percentage in relation to those that are genuine reflect some of the more subtle aspects of spectral processing. These include the smallest distance among the poles and zeros, the density of poles and zeros in the complex plane, and also inter-separations among poles and zeros [16]. The Argand plots, as displayed for the present problem in panels (i) and (ii) of Fig. 2, show that all the physical poles are lined up at infinitesimally small distances below the real axis which is characterized as $\mathrm{Re}\,\nu = 0$. Widths are inversely proportional to the corresponding lifetimes of resonances. As such, horizontally aligned poles in the immediate neighborhood of zero-valued chemical shifts on Fig. 2 are associated with long-lived resonances. Longevity implies stability and robustness against external perturbations, such as noise. The spectral zeros of the physical resonances contribute to the overall stability. As per Eq. (8), the distance between a given genuine pole and the associated genuine zero is proportional to the peak height. However, the factor of proportionality is a quite involved function of the peak widths for *all* the K genuine resonances, as is clear from Eq. (7).

As explained in the Introduction of this paper, and demonstrated in numerous previous applications [6,8,14,16], after the point of convergence, Padé-reconstructions remain stable, since all the additional resonances are readily recognized as being non-physical, by way of the SNS concept implemented through detection of Froissart doublets. In other words, K as the number of genuine resonances, is treated as an unknown parameter and determined uniquely through the FPT. It should also be emphasized that the stability of the FPT sharply contrasts with most other parametric estimators that typically show wild oscillations before eventually converging, if at all [6,8,14].

Besides determining K, the $\mathrm{FPT}^{(-)}$ exactly reconstructs the four other real-valued spectral parameters, namely the two complex-valued frequencies and complex amplitudes for all twelve metabolite peaks, in the presence of realistic background noise. This required only 128 signal points, and such a finding is even more remarkable than convergence of the total shape spectrum. Thereby, the most essential clinical information, which is the metabolite concentrations, was computed unequivocally. By applying in vitro MRS with high magnetic field strength, as well as sophisticated laboratory processing techniques, several MR-visible compounds have been identified that help distinguish benign and cancerous ovarian lesions [13,17–19]. Herein, we see that Padé reconstruction holds promise for detecting and accurately quantifying these compounds in the presence of realistic background noise.

Our initial analyses were performed using noise-free synthesized time signals to set up the fully-controlled standard for the FPT in the case of the first application of this method to data within the realm of ovarian cancer diagnostics by MRS [11,12].

This was methodologically justified [14]. In the present study we extend our analysis to noise-corrupted synthesized ovarian data (still well-controlled), as a key step in the validation process for Padé-optimized MRS. The next step, which is in progress, is to perform analysis with the FPT upon in vivo encoded MR-time signals from benign and malignant lesions of the ovary, with in vitro and in vivo clinical correlations together with histopathology for validation.

Massuger et al. [17] consider that in vivo MRS could become the method of choice for early stage ovarian cancer detection, insofar as the obstacles hindering the acquisition of high quality time signals and subsequent reliable analysis of spectra as well as their interpretation can be surmounted. The results presented in this paper suggest that Padé-optimized MRS could contribute to this aim.

Effective strategies for accurately detecting ovarian cancer in its early stages are urgently needed. Given that MR-based modalities do not entail exposure to ionizing radiation, insofar as their diagnostic accuracy were improved, magnetic resonance imaging and spectroscopy could have more widespread application in screening surveillance for early ovarian cancer detection. Padé-optimized MRS could help achieve that goal.

5 Conclusion

In the presence of realistic background noise, the FPT applied to time signals generated according to in vitro MRS data as encoded from malignant ovarian cyst fluid showed high resolution and accurately reconstructed spectral parameters for all the genuine resonances. Thereby, the FPT provided fully reliable estimates of metabolite concentrations characteristic of malignant ovarian cyst fluid. The powerful concept of SNS through the identification of pole-zero coincidences (Froissart doublets) is illustrated in a setting which is directly relevant to cancer diagnostics. In vivo MRS has been envisioned as the potential method of choice for early stage ovarian cancer detection. However, this would require overcoming the barriers obstructing the acquisition of high quality time signals and subsequent trustworthy analysis of spectra. Molecular imaging through magnetic resonance spectroscopy could therefore have much broader applications in screening surveillance for early ovarian cancer detection, particularly among women at high risk. This possibility is especially attractive because there is no exposure to ionizing radiation through magnetic resonance. The results of the present study strongly suggest that Padé-optimization will be an invaluable step towards improving the diagnostic accuracy of MRS for ovarian cancer. Thereby, better outcomes can be anticipated for women afflicted with this malignancy.

Acknowledgments This work was supported by Cancerfonden, King Gustav the 5th Jubilee Fund and the Karolinska Institute Research Fund and COST MP1002 "Nano-scale insight in ion beam cancer therapy" to which the authors are grateful.

References

1. S. Pecorelli, G. Favalli, L. Zigliani, F. Odicino, Cancer in women. Int. J. Gynaecol. Obstet. **82**, 369–379 (2003)

2. M.A. Brewer, K. Johnson, M. Follen, D. Gershenson, R. Bast, Prevention of ovarian cancer: intraepithelial neoplasia. Clin. Cancer Res. **9**, 20–30 (2003)
3. E.R. Woodward, H.V. Sleightholme, A.M. Considine, S. Williamson, J.M. McHugo, D.G. Cruger, Annual surveillance by CA125 and transvaginal ultrasound for ovarian cancer in both high-risk and population risk women is ineffective. B.J.O.G. **114**, 1500–1509 (2007)
4. S.S. Buys, E. Partridge, M.H. Greene, P.C. Prorok, D. Reding, T.L. Riley, P. Hartge, R.M. Fagerstrom, L.R. Ragard, D. Chia, G. Izmirlian, M. Fouad, C.C. Johnson, J.K. Gohagan The Team PLCO Project, Ovarian cancer screening in the Prostate, Lung, Colorectal and Ovarian (PLCO) cancer screening trial: Findings from the initial screen of a randomized trial. Am. J. Obstet. Gynecol. **193**, 1630–1639 (2005)
5. K. Kinkel, Y. Lu, A. Mehdizade, M.-F. Pelte, H. Hričak, Indeterminate ovarian mass at US: incremental value of second imaging test for characterization—Meta-analysis and Bayesian analysis. Radiology **236**, 85–94 (2005)
6. Dž. Belkić, K. Belkić, *Signal Processing in Magnetic Resonance Spectroscopy with Biomedical Applications* (Taylor & Francis Publishers, London, 2010)
7. Dž. Belkić, Strikingly stable convergence of the fast Padé transform (FPT) for high resolution parametric and non-parametric signal processing of Lorentzian and non-Lorentzian spectra. Nucl. Instr. Meth. Phys. Res. A **525**, 366–371 (2004)
8. Dž. Belkić, *Quantum Mechanical Signal Processing and Spectral Analysis* (Taylor & Francis Publishers, London, 2005)
9. Dž. Belkić, K. Belkić, Unequivocal disentangling genuine from spurious information in time signals: Clinical relevance in cancer diagnostics through magnetic resonance spectroscopy. J. Math. Chem. **44**, 887–912 (2008)
10. Dž. Belkić, K. Belkić, The general concept of signal-noise separation (SNS): Mathematical aspects and implementation in magnetic resonance spectroscopy. J. Math. Chem. **45**, 563–597 (2009)
11. K. Belkić, Resolution performance of the fast Padé transform: Potential advantages for magnetic resonance spectroscopy in ovarian cancer diagnostics. Nucl. Instr. Meth. Phys. Res. A **580**, 874–880 (2007)
12. Dž. Belkić, K. Belkić, Mathematical modeling applied to an NMR problem in ovarian cancer detection. J. Math. Chem. **43**, 395–425 (2008)
13. E.A. Boss, S.H. Moolenaar, L.F.A.G. Massuger, H. Boonstra, U.F. Engelke, J.G. de Jong, R.A. Wevers, High-resolution proton nuclear magnetic resonance spectroscopy of ovarian cyst fluid. NMR Biomed. **13**, 297–305 (2000)
14. Dž. Belkić, Exact quantification of time signals in Padé-based magnetic resonance spectroscopy. Phys. Med. Biol. **51**, 2633–2670 (2006)
15. Dž. Belkić, K. Belkić, The potential for practical improvements in cancer diagnostics by mathematically-optimized magnetic resonance spectroscopy. J. Math. Chem. **49**, 2408–2440 (2011)
16. Dž. Belkić, Exact signal-noise separation by Froissart doublets in the fast Padé transform for magnetic resonance spectroscopy. Adv. Quantum Chem. **56**, 95–179 (2009)
17. L.F.A.G. Massuger, P.B.J. van Vierzen, U.F. Engelke, A. Heerschap, R.A. Wevers, 1H-magnetic resonance spectroscopy: a new technique to discriminate benign from malignant ovarian tumors. Cancer **82**, 1726–1730 (1998)
18. I.C. Smith, D.E. Blandford, Diagnosis of cancer in humans by 1H NMR of tissue biopsies. Biochem. Cell. Biol. **76**, 472–476 (1998)
19. J.C. Wallace, G.P. Raaphorst, R.L. Somorjai, C.E. Ng, M. Kee Fung Fung, M. Senterman, I.C. Smith, Classification of 1H MR spectra of biopsies from untreated and recurrent ovarian cancer using linear discriminant analysis. Magn. Reson. Med. **38**, 569–576 (1997)